COPY 2

TECHNICAL MEMORANDUM

X-470

INVESTIGATION OF THE PERFORMANCE AND CONTROL

OF A MACH 3.0, TWO-DIMENSIONAL, EXTERNAL-

INTERNAL-COMPRESSION INLET

By David N. Bowditch and Bernhard H. Anderson

Lewis Research Center
Cleveland, Ohio

1961

NATIONAL AERONAUTICS AND SPACE ADMINISTRATION

WASHINGTON   June 1961

NATIONAL AERONAUTICS AND SPACE ADMINISTRATION

TECHNICAL MEMORANDUM X-470

INVESTIGATION OF THE PERFORMANCE AND CONTROL OF A

MACH 3.0, TWO-DIMENSIONAL, EXTERNAL-

INTERNAL-COMPRESSION INLET*

By David N. Bowditch and Bernhard H. Anderson

SUMMARY

An experimental investigation of a Mach 3.0, two-dimensional, external-internal-compression inlet feeding three engines was conducted over a Mach number range from 2.0 to 2.98 at angles of attack from 0° to 4°. At Mach 2.98, a maximum total-pressure recovery of 0.89 was obtained at a mass-flow ratio of 0.88. Recovery, in general, increased as Mach number decreased, and reached a value of 0.93 at Mach 2.00. Since the inlet was shielded under a stub wing, the recovery decrease due to a 4° angle of attack was never more than 1.5 counts over the Mach number range.

Inlet controls were investigated, and it was determined that the inlet throat height could be scheduled as a function of the first-ramp Mach number only and that conditions near peak recovery could be set by positioning the bypass to keep a constant throat-exit Mach number.

INTRODUCTION

A wind tunnel investigation was conducted at Mach numbers from 2.0 to 2.98 and angles of attack to 4° on a two-dimensional, external-internal-contraction inlet designed for Mach 3.0. The inlet tested was one-half of an induction system consisting of two, two-dimensional inlets mounted back to back and each feeding three engines. The inlets were positioned vertically so that they initially compress outward, and were mounted centrally under a delta wing so that they were shielded from flow angularity across the upper and lower plates. Performance data are presented for the optimum internal boundary-layer bleed system investigated; additionally, the study included the steady-state effects of engine-out operation on the two remaining ducts. Control parameters for positioning both the throat height and bypass were investigated, and usable control parameters are presented.

*Title, Unclassified.

CONFIDENTIAL

E-1073

SYMBOLS

A   area, sq ft

A_{cl} cowl-lip area, sq ft

A_{th} throat area, sq ft

h_{cl} cowl-lip height (horizontal component, perpendicular to the free stream, of distance between cowl lip and first-ramp leading edge), 1.787 ft

h_{th} throat height (minimum distance between throat ramp and cowl), ft

M   Mach number

m   mass flow, slugs/sec

P   total pressure, lb/sq ft

$\bar{P}$ average total pressure, lb/sq ft

ΔP_2 maximum total pressure minus minimum total pressure at engine-face station, lb/sq ft

P_{th} total pressure at the throat, lb/sq ft

p   static pressure, lb/sq ft

p_s sensor pressure used for control signal pressure ratio, lb/sq ft

Re   Reynolds number

x   distance downstream of cowl lip, ft

α angle of attack, deg

θ_{3R} third-ramp angle (angle with respect to free-stream direction), deg

Subscripts:

c   center engine

cs   cowl-side engine

r   ramp-side engine

1R   first ramp

CONFIDENTIAL

3R   third ramp

O   free-stream conditions

2   engine-face station

APPARATUS AND PROCEDURE

Figure 1 shows the model installed in the 10- by 10-foot supersonic wind tunnel. The forward portion (fig. 1(a)) is a quarter-scale model of one-half of the actual induction system, which includes two vertical inlets placed back to back. Each inlet supplied three engines in the prototype. The lower plate is behind the Mach wave emanating from the wing at Mach 3.0 and 0° angle of attack. The upper-plate leading edge was located below the wing to remove the wing boundary layer. Figure 1(b) shows the flow-metering section and presents a picture of the overall length of the model, which was 42.5 feet.

A schematic diagram of the inlet is presented in figure 2. The first two compression surfaces were fixed ramps inclined to the free stream at angles of 7° and 12°. The third ramp could be varied remotely from 12° to 17.5^O with respect to the free stream. The throat (fifth) ramp was actuated so that it remained at a constant angle with respect to the cowl. The fourth ramp was a free moving surface, and its position was determined by the positions of the third and throat ramps. The sixth ramp faired between the throat ramp and the fixed subsonic diffuser ramp through a fixed joint at the throat ramp and a sliding joint to the diffuser; this allowed for changes in the axial length of the movable surfaces. The cowl was a flat compression surface in the supersonic portion of the inlet and was inclined 6° to the free stream.

Figure 3 presents a schematic diagram of the bleed configuration tested and shows the areas of bleed on each surface. Provisions were made for area bleed on the third, fourth, and throat ramps and on the side walls and cowl. The bleed passages for the movable ramps were compartmented to preclude recirculation and were ducted to the free stream. The cowl and the side-wall bleed flows were dumped directly into the free stream.

The variation in internal contraction with throat height is presented in figure 4. A schematic diagram of the model in figure 5 shows the inlet, bypass, engine-face, and flow-metering stations. The bypass flow required for inlet-engine matching leaves the main duct through perforations just ahead of each of the three engine faces. Each engine face was instrumented with four 5-tube, area-weighted rakes, 90° apart. The center tube on each rake contained a pitot static tube. Total-pressure recoveries and distortions were calculated from these rakes.

Where only one distortion is presented, it is the highest of the three individual engine-face distortions. Downstream of the engine faces, the flow was diffused, straightened by screens, and measured by ASME nozzles. Four static taps were located upstream of each nozzle and four at each throat. These statics were used in the mass-flow calculations. Each engine flow was controlled by a choked plug downstream of the nozzle.

Pressure distributions along the cowl were obtained from a row of static orifices along the centerline of the cowl. A four-tube rake, located at the throat, was used to obtain the total pressure for use as a control reference. The first ramp was instrumented with three static orifices and two total-pressure tubes to determine local Mach number. Diffuser-exit static pressure was measured just upstream of the point where the main duct separated into the three engine ducts.

The inlet was tested at Mach numbers from 2.0 to 2.98, angles of attack from $0°$ to $4°$, and Reynolds numbers of 0.50×10^6 to 2.5×10^6 per foot. The unstart throat height was determined by decreasing the throat height until the inlet unstarted, with the mass-flow metering plugs at maximum flow area. The peak recovery of the inlet at a given throat height was determined by first determining the plug area that just unstarted the inlet and then setting 100.5 percent of that plug area.

RESULTS AND DISCUSSION

Inlet Performance

Figure 6 presents peak inlet performance for third-ramp angles of $16.5°$, $15.5°$, and for the angle of maximum recovery. Only the peak recovery conditions are presented for a range of throat heights. Angle-of-attack data are presented for optimum throat heights only.

Figure 6(a) presents inlet performance data for a third-ramp angle of $16.5°$, which is the optimum third-ramp angle for Mach 3.0 operation. At Mach 2.98, a peak pressure recovery of 0.89 was obtained at a mass-flow ratio of 0.88 and a distortion level of 0.025. The inlet performance was relatively insensitive to throat height; for example, at Mach 2.98 where the effect was largest, increasing the throat height parameter (h_{th}/h_{cl}) from 0.23 to 0.244 (6 percent) decreased total-pressure recovery less than 1 percent. The peak pressure recovery was fairly constant with Mach number, staying just above the 90-percent level at Mach numbers from 2.78 to 2.18. No data are presented at Mach 2.0 because the high third-ramp angle $(\theta_{3R} = 16.5°)$ caused the oblique shock to detach from the cowl lip. Therefore, no inlet unstarting occurred, and peak recovery as defined in APPARATUS AND PROCEDURE could not be

determined. The inlet distortion increased from a low of 0.022 at Mach 2.98 to 0.10 at Mach 2.18, which was at least partially due to the corresponding increase in engine-face Mach number from 0.249 to 0.49. The mass-flow ratio decreased continuously with Mach number from 0.88 at Mach 2.98 to 0.73 at Mach 2.18. Because the inlet was shielded from angle of attack by a wing, the reduction in recovery due to angle of attack was limited to a maximum of 1.5 counts at 4°, and the distortion was unaffected. The increased mass flow at angle of attack was caused by precompression from the wing.

Reducing the third-ramp angle to 15.5^O (fig. 6(b)) improved total-pressure recovery 2 counts at Mach 2.58 and 1 count at Mach 2.18, and caused only a minor reduction in recovery of 0.3 count at Mach 2.98. Data are presented at Mach 2.0 for a third-ramp angle of 15.5^O, since the oblique shock did not detach from the cowl as it did with a third-ramp angle of 16.5^O. Changing the third-ramp angle from 16.5^O to 15.5^O did not affect distortion. Mass-flow ratios are not presented at a third-ramp angle of 15.5^O because the bypass was not sealed, thus allowing a small but unknown amount of flow to leak out the closed bypass.

Inlet performance at the third-ramp angle for maximum recovery for each Mach number is presented in figure 6(c). These settings of 16.5^O, 13.5^O, 12°, and 12° at corresponding Mach numbers of 2.98, 2.58, 2.18, and 2.00 resulted in gains of about 2 counts in total-pressure recovery at Mach numbers other than Mach 2.98 when compared with data obtained at a ramp angle of 16.5^O (fig. 6(a)). Only slight increases in mass-flow ratio were encountered at the lower Mach numbers and low third-ramp angles. When compared with the peak recoveries at a constant third-ramp angle of 15.5^O, it can be seen that significant gains in pressure recovery are obtained at Mach 2.0 only by setting the lower third-ramp angle.

Figure 7 presents a summary of variation of peak inlet recovery with third-ramp angle. At Mach 2.98 and 2.58, a maximum inlet pressure recovery occurred at third-ramp angles of 16.5^O and 13.5^O, respectively. However, the peak inlet pressure recovery was relatively insensitive to the third-ramp angle, as the recovery remains within a count of the peak value over a range of at least 3°. A peak in the curve of inlet pressure recovery as a function of third-ramp angle did not occur at Mach 2.18 and 2.00, even when the third ramp was lowered to the same angle (12°) as the second, fixed ramp.

Total-pressure contours at the compressor-face stations are presented in figure 8. There is little distortion at peak pressure recovery at Mach 2.98, as can be seen from figure 8(a). At Mach 2.18 and a third-ramp angle of 16.5^O, where the compressor-face Mach number is double the Mach 2.98 value, the distortion is greatly increased (fig. 8(b)). The high recovery air tends to stay near the center of the duct

and enters the center engine, while the duct boundary layer appears on the bottom and top of the center engine and on the outer sides of both the cowl- and ramp-side engines. The ramp-side engine-face recovery was generally lowest; this was probably due to the curvature of the ramps. By reducing the third-ramp angle to 12° at Mach 2.18 (fig. 8(c)), the recovery was increased at both the ramp-side and center engine faces but decreased at the cowl-side engine face. A high recovery flow appears to have moved from the right of the inlet to the center, as if separation had been stopped (this will be shown later). When the bypass was opened to simulate actual flight conditions (fig. 8(d)), the distortion was reduced by removal of the air around the periphery of the engine ducts.

Inlet performance at the individual engine faces is presented in figure 9. The center engine always had the highest total-pressure recovery by 2 to 4 counts. At high third-ramp angles and low Mach numbers, the low recovery at the ramp-side engine face appears to be due to a separation, as the duct total pressure is much lower than the total pressure in the center- and cowl-side ducts, and the variation with Mach number is very similar to the variation of diffuser-exit static pressure. However, this separation does not appear at the third-ramp angle of 12°, where the ramp- and cowl-side engine-face recoveries are almost the same. The distortion for the center engine was always less than the cowl- and ramp-side engines, which were similar in nature.

The effect of reducing the Mach number at one engine face, simulating engine-out conditions, on the recovery and distortion at the other two engine faces is shown in figure 10. The engine-face Mach numbers of the full flowing ducts are those corresponding to flight conditions, and the excess air was diverted through the bypass. At Mach 2.18, reduction of the ramp-side engine-face Mach number (fig. 10(a)) forced its low recovery flow into the center engine, thus reducing the pressure recovery and increasing the distortion of the center engine. Some of the high recovery flow that usually entered the center engine raised the pressure recovery of the cowl-side engine face. Reduction in the center or the cowl-side engine-face Mach numbers (figs. 10(b) and (c)) had little effect on the conditions at the other engine faces. Further, there was little effect of alternately reducing the engine-face Mach numbers at a free-stream Mach number of 2.98. Therefore, there seems to be no deterioration in engine-face flow under simulated engine-out conditions, unless poor flow already is present somewhere in the duct.

The effect of Reynolds number on peak inlet performance is presented in figure 11. By reduction of the Reynolds number from 2.5×10^6 to 0.5×10^6, the total-pressure recovery was reduced about 2.5 counts, the mass-flow ratio dropped about 2.5 counts, and the distortion increased slightly. The ratio of static pressure on the first ramp to the free-stream static pressure was higher at the lower Reynolds number,

E-1073

indicating a larger effective ramp angle, which would spill flow and thereby reduce the captured mass flow. Other inlets employing internal contraction have been investigated at intermediate Reynolds numbers in the 10- by 10-foot tunnel (ref. 1), and the recovery has been found to be relatively constant down to Reynolds numbers of 1.0 to 1.5×10^6 per foot and then to decrease. A similar variation would be expected for this inlet.

Since only peak recovery data have been introduced, figure 12 is presented to illustrate the mass-flow variation with recovery and the effect of the throat height on the shape of the pressure-recovery - mass-flow curve. At a throat height of 100.5 percent of the unstart value, the terminal-shock position had little effect on the static pressures ahead of the throat where the porous bleed is located, so that recovery changed at nearly constant mass-flow ratio. However, at larger throat areas, the shock position increased the throat static pressures, which increased the bleed and caused the mass flow to decrease as the pressure recovery was increased. This "bending over" of the pressure-recovery - mass-flow curve is advantageous from a control standpoint in that it furnishes a change in control parameter at nearly constant pressure recovery.

The variation in the unstart and restart throat height with free-stream Mach number is presented in figure 13. The predicted restart throat height is based on the ability of the throat to pass all the capture mass flow, with the terminal shock right at the cowl lip. This criterion, however, is not the case, since the actual restart throat heights fall well below the predicted values. This is due to an increase in the porous bleed during starting as well as a condition previously described in reference 2. In that report, it was observed that a separation on the external compression surface caused an oblique shock which spilled flow around the cowl lip and improved the efficiency of compression. Both results decrease the required throat area for starting. Because of these effects, the predicted value is quite conservative. Transient starting conditions reducing the required change in exit area, were illustrated during the test by reducing and then increasing the flow with the throat height at the restart position, which retained a large amount of internal contraction. As the exit area was reduced, the pressure recovery was increased until the inlet unstarted and entered buzz. When the exit area was increased slightly, the inlet was found to be started and at peak pressure recovery as soon as the inlet buzz stopped. Under steady-state conditions, the exit area would have to be greatly increased to allow all the flow to pass at the low recovery starting conditions. Inlet starting during buzz, however, was rather erratic and hence was not thoroughly investigated.

Inlet Control Parameters

Inlet control parameters must be found to regulate both the amount of internal contraction and bypass weight flow. The first-ramp Mach number is a possible parameter for positioning the throat panel (fig. 14). In this case the static and total pressures on the first ramp could be measured, and the control would schedule throat height with the ratio of the pressures. At 0° angle of attack the unstart throat height varies smoothly with the first-ramp Mach number. At angle of attack, the throat heights fall below the 0° curve, thus showing the ability to set the optimum schedule of throat height with first-ramp Mach number at 0° angle of attack without unstarting the inlet at higher angles of attack. The first-ramp pressures, however, have a low gain and may be difficult to sense.

Static-pressure variation in the throat region could possibly be used for control of both the inlet contraction, or throat height, and the terminal-shock or bypass position. It has been proposed to control the inlet contraction by measuring the throat supersonic Mach number by sensing the throat total and static pressures. For control, the throat height would be reduced until the throat Mach number reached some minimum value. However, such a control requires the pressures to be a function of external conditions only; and it can be seen in figure 15 that the terminal shock affects the static pressure throughout the throat region, so that such a control does not appear to be feasible.

For terminal-shock or bypass control, the static-pressure rise associated with the terminal shock is the most obvious control parameter. However, for this control, the peak recovery station for the terminal shock must be consistent, so that the pressure rise can be measured in a fixed region of the throat near peak recovery. But in figure 15 it can be seen that the shock position at peak recovery changed significantly with a rather minor change in throat height (102 to 108 percent of the unstart throat height). For this reason, measuring the full shock pressure rise for shock position control over a wide range of flight conditions does not appear feasible. However, the static-pressure variation at the station marked "sensor" varies quite consistently at both throat heights, and for this reason the static pressure at that position was investigated for use as a possible control parameter.

The performance of a recovery control parameter consisting of the ratio of the static pressure at the station marked "sensor" (fig. 15) to a total pressure at the throat is presented in figures 16 to 18. Figure 16 presents the variation in the control parameter with recovery change at the third-ramp angle for maximum recovery and Mach numbers of 2.98, 2.58, and 2.18. A single pressure ratio of 0.67 will position the shock within a maximum of 2 counts of peak pressure recovery for all conditions presented, except at 100.5 percent of the unstart throat

height. For other third-ramp angles (fig. 17), the data indicate similar performance for the same pressure ratio of 0.67 at all conditions except at 110 percent of the unstart throat height and Mach 2.18. Figure 18 presents the effect of 4° angle of attack on the performance of the control signal pressure ratio. A constant pressure ratio of 0.67 again was found to work satisfactorily except at Mach 2.98, where this value was not reached. However, the problem at Mach 2.98 and 4° angle of attack possibly could be solved by choosing a different station to sense static pressure. The largest problem that can be foreseen in using this control parameter, which is based on setting a constant Mach number downstream of the throat, is that it has a much lower gain than if a shock pressure rise were to be sensed. The throat-exit Mach number appears to have general application as a recovery control parameter, since it also was found to be usable for control of an axially symmetric, internal-contraction inlet employing flush slot bleed (ref. 3). The performance has been discussed for use of a constant control pressure ratio over the Mach number range investigated, but this performance could be improved by scheduling a ratio as a function of free-stream conditions.

SUMMARY OF RESULTS

A Mach 3.0, two-dimensional, external-internal-compression inlet supplying three engines was tested in the 10- by 10-foot supersonic wind tunnel at Lewis Research Center with the following results:

1. A total-pressure recovery of 0.89 was obtained at a mass-flow ratio of 0.88 at Mach 2.98.

2. Near-optimum inlet performance could be obtained with a constant inlet third-ramp angle of 15.5° over the Mach number range from 2.0 to 3.0.

3. Decreasing the Reynolds number from 2.5×10^6 to 0.5×10^6 per foot reduced the peak pressure recovery 2.5 counts and the mass-flow ratio 2.5 counts.

4. Reducing the flow in any of the three engine ducts to simulate engine-out conditions affected the flow in the other engine ducts only if considerable distortion were already present at the diffuser exit.

5. The inlet throat height can be satisfactorily scheduled as a function of first-ramp Mach number.

6. The terminal shock affected the static pressure upstream of the throat. It was therefore impossible to sense a throat Mach number for use as a parameter to position the throat height.

7. The terminal shock system was not discrete at peak pressure recovery, and its location in the duct at peak recovery varied with Mach number and throat height. This made it impossible to sense the full terminal-shock pressure rise at one station at or near peak recovery.

8. Using the throat-exit Mach number (by setting a ratio between a throat-exit static and a throat total) as a bypass control parameter appeared feasible.

Lewis Research Center
National Aeronautics and Space Administration
Cleveland, Ohio, January 27, 1961

REFERENCES

1. Samanich, N. E., Barnett, D. O., and Salmi, R. J.: Effect of External Boundary Layer on Performance of Axisymmetric Inlet at Mach Numbers of 3.0 and 2.5. NASA TM X-49, 1959.

2. Bowditch, David N., and Anderson, Bernhard H.: Performance of an Isentropic, All-Internal-Contraction, Axisymmetric Inlet Designed for Mach 2.50. NACA RM E58E16, 1958.

3. Bowditch, David, Anderson, Bernhard H., and Tabata, William: Performance and Control of a Full-Scale, Axially Symmetric, External-Internal-Compression Inlet from Mach 2.0 to 3.0. NASA TM X-471, 1961.

E-1073

E-1073

C-52617
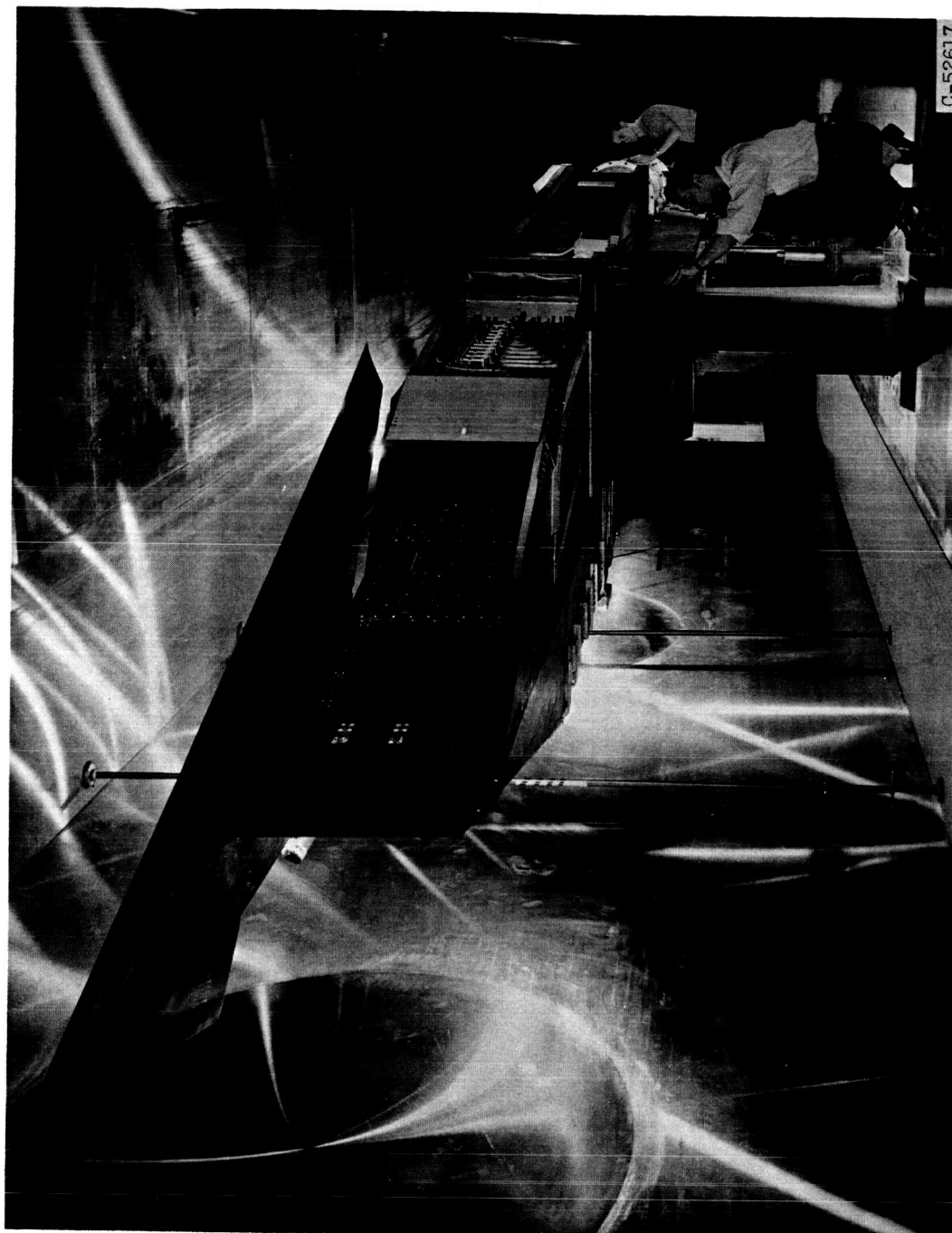
(a) View from upstream showing inlet and stub wing.

Figure 1. - Model installed in 10- by 10-foot tunnel.

E-1073

C-52752
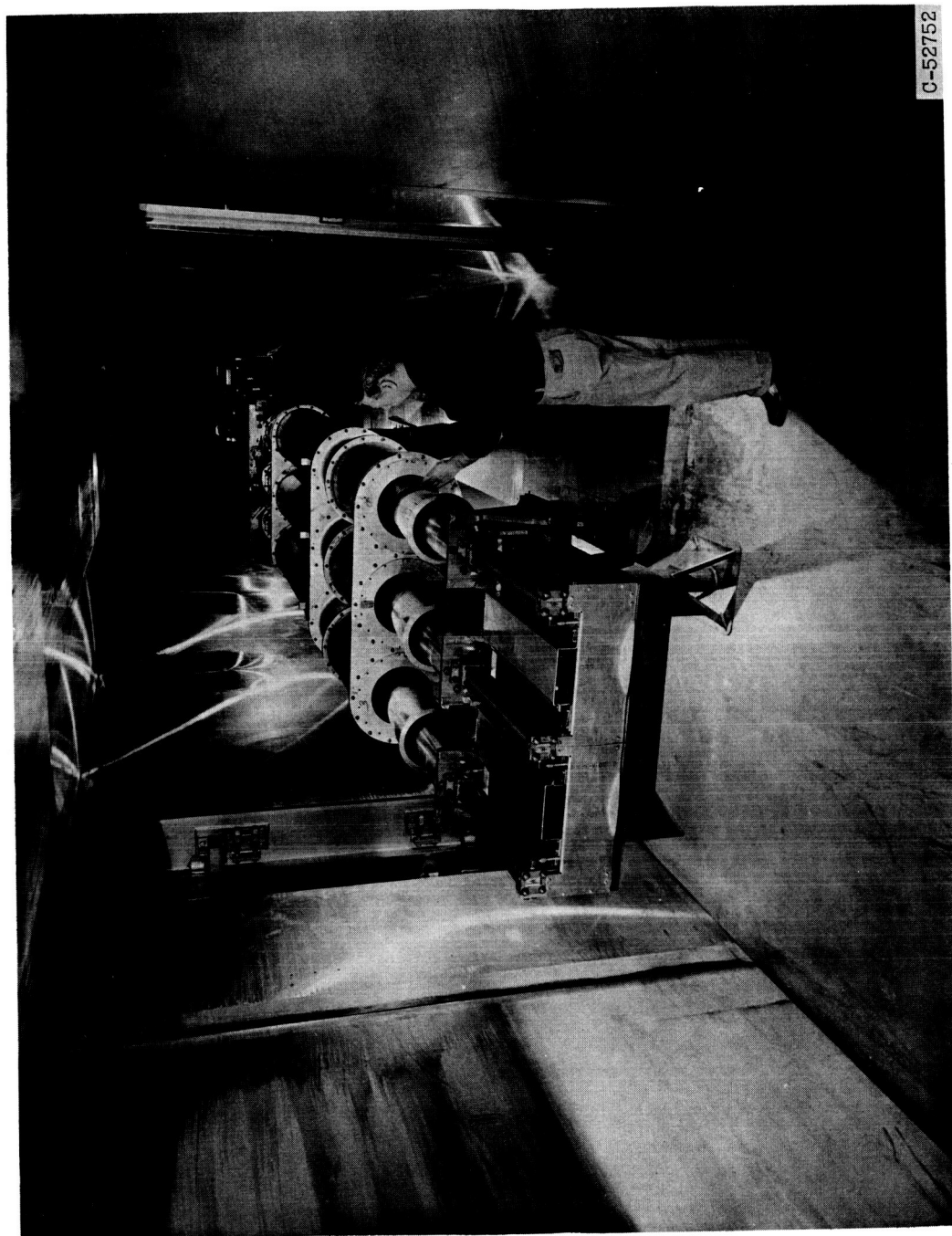
(b) View from downstream showing flow-metering section.

Figure 1. - Concluded.   Model installed in 10- by 10-foot tunnel.

E-1073

CD-6992

Sixth ramp

Throat ramp (fifth)

Upper plate

Lower plate

Fourth ramp

Wing boundary-layer bleed slot

Fixed pins

Porous material

Third ramp

Second ramp

Stub wing

First ramp
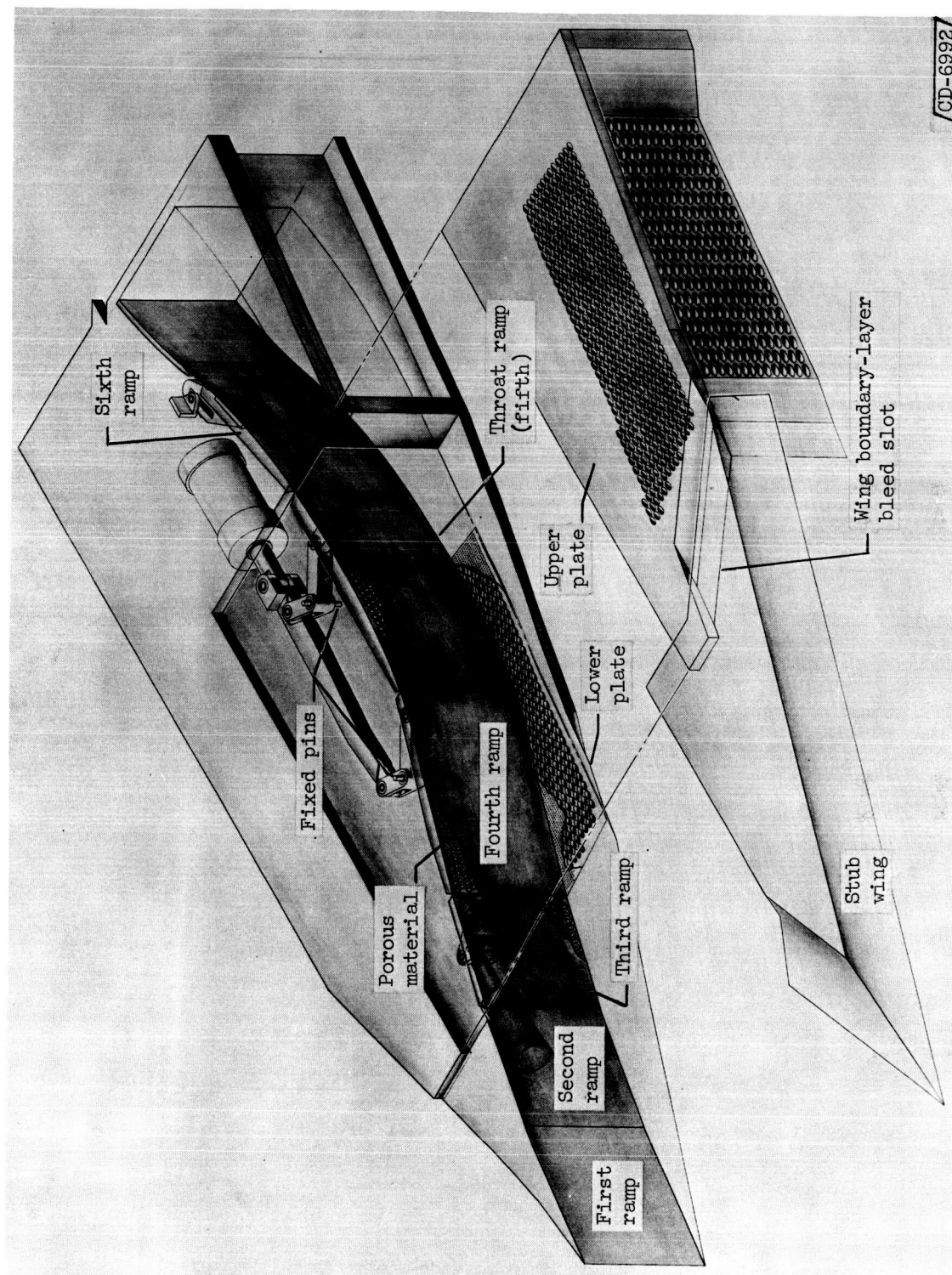
Figure 2. - Inlet.
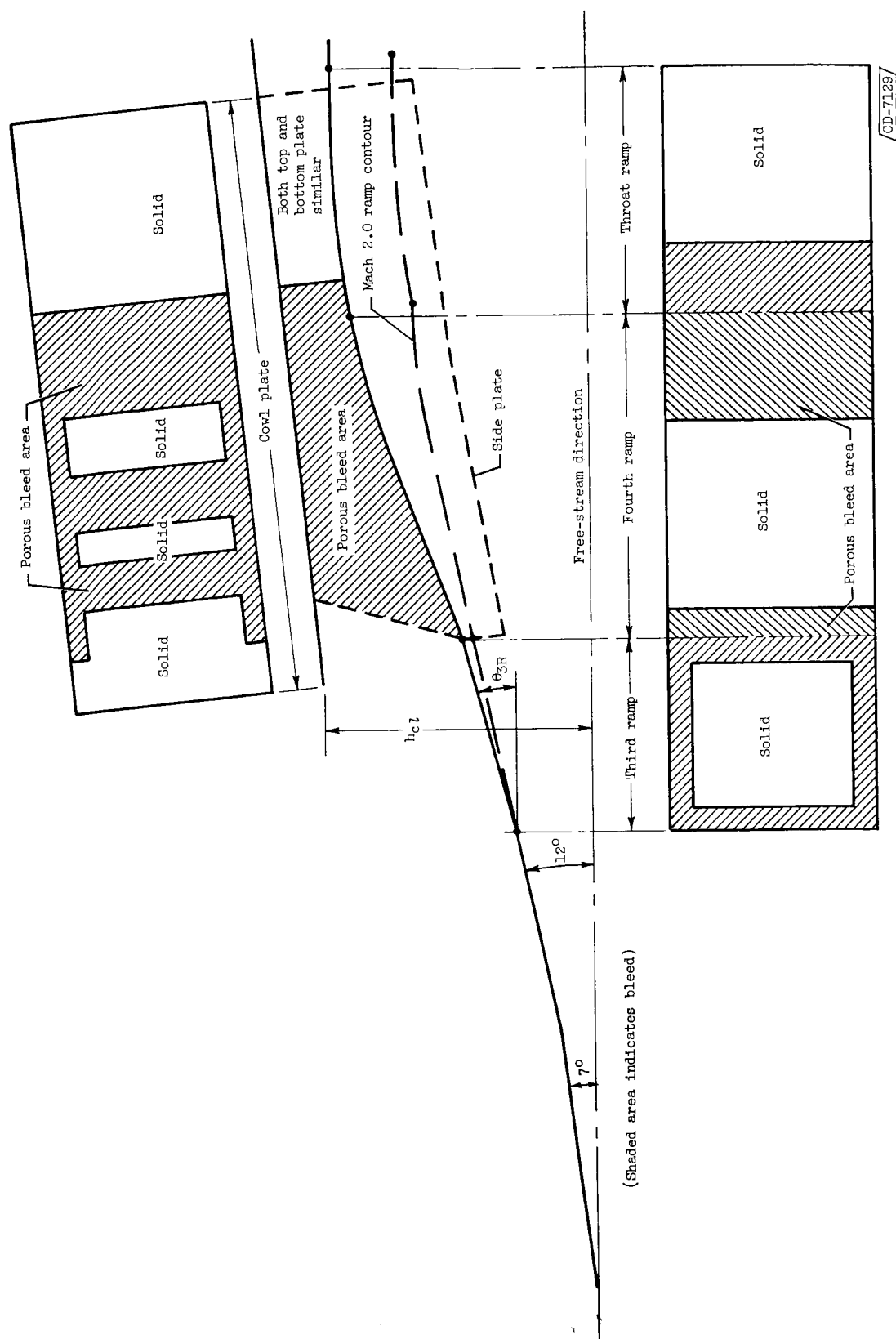
Figure 3. - Bleed configuration.
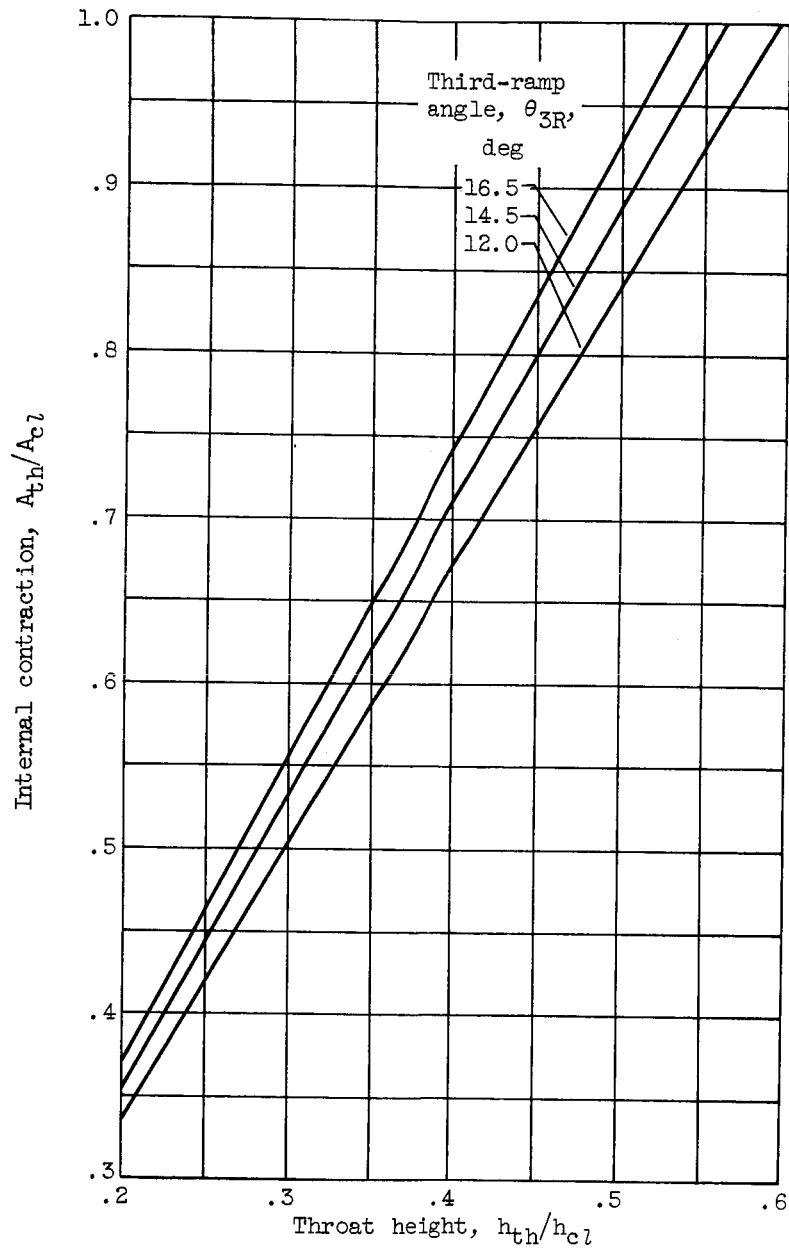
Figure 4. - Relation between internal contraction
and throat height.
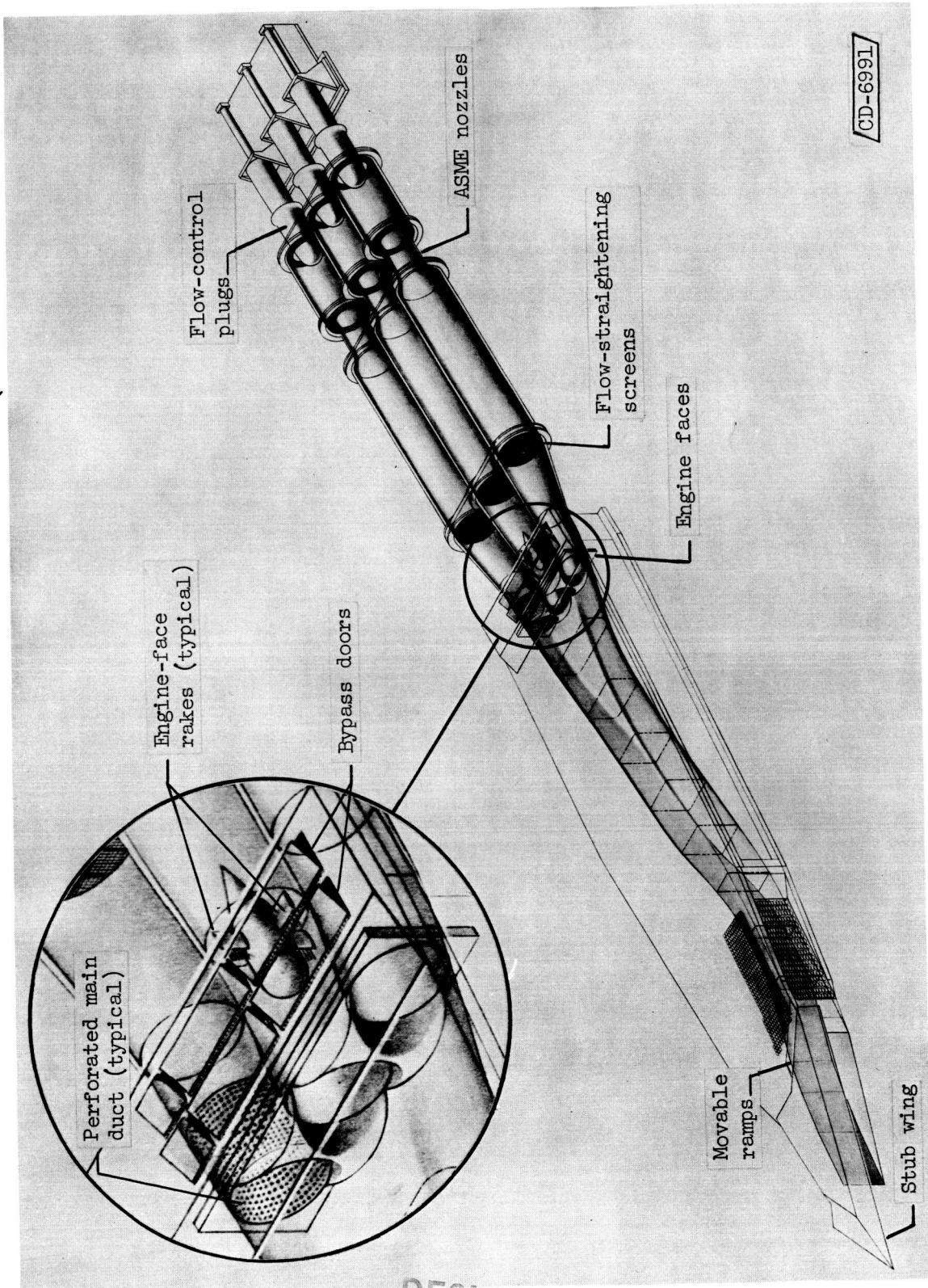
Figure 5. - Inlet model.

E-1073

CD-6991

Flow-control plugs

ASME nozzles

Flow-straightening screens

Engine faces

Engine-face rakes (typical)

Bypass doors

Perforated main duct (typical)

Movable ramps

Stub wing

E-1073
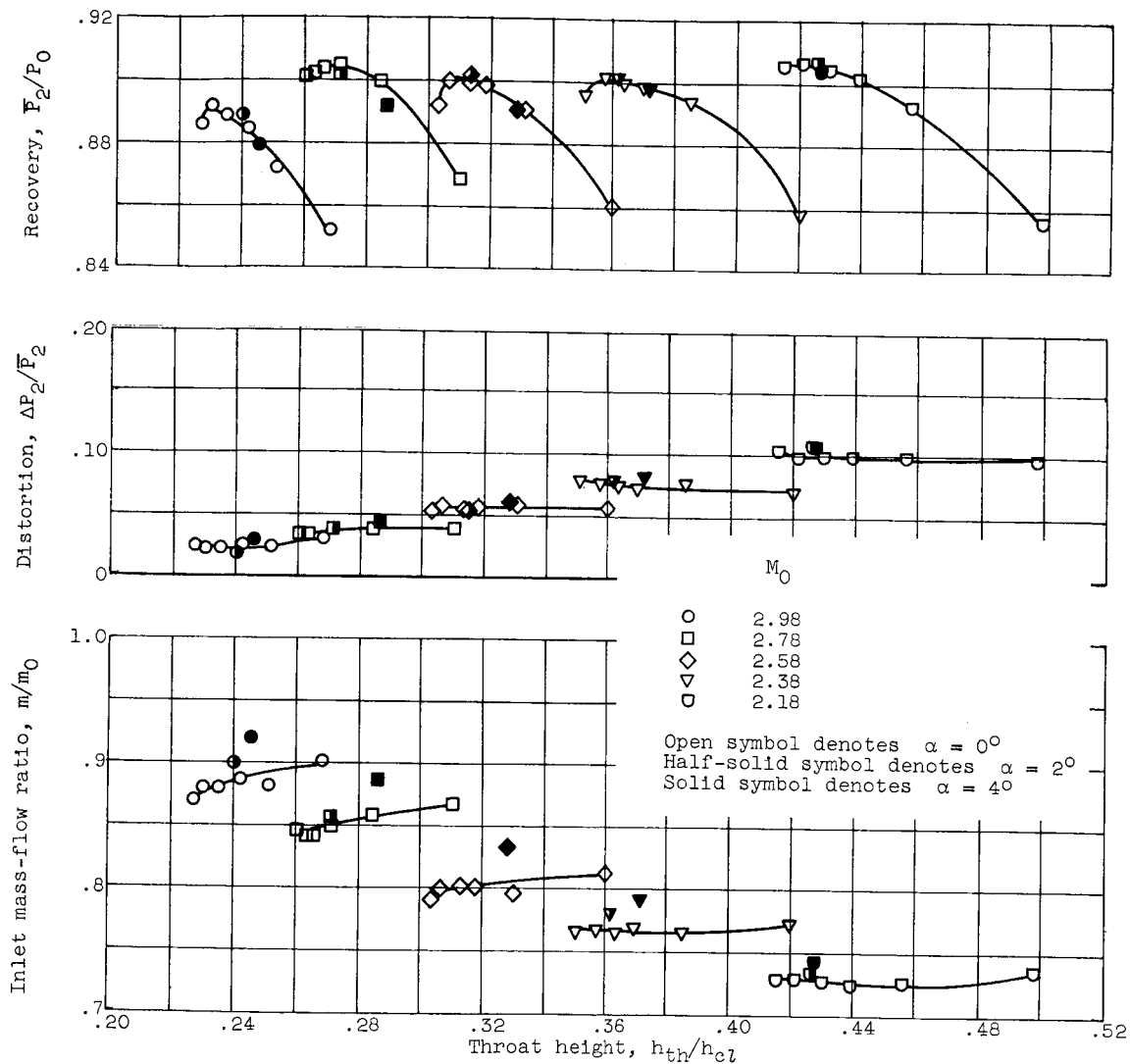
(a) Third-ramp angle, 16.5° (bypass sealed).

Figure 6. - Peak inlet performance. Reynolds number, 2.5×10⁶ per foot.

18
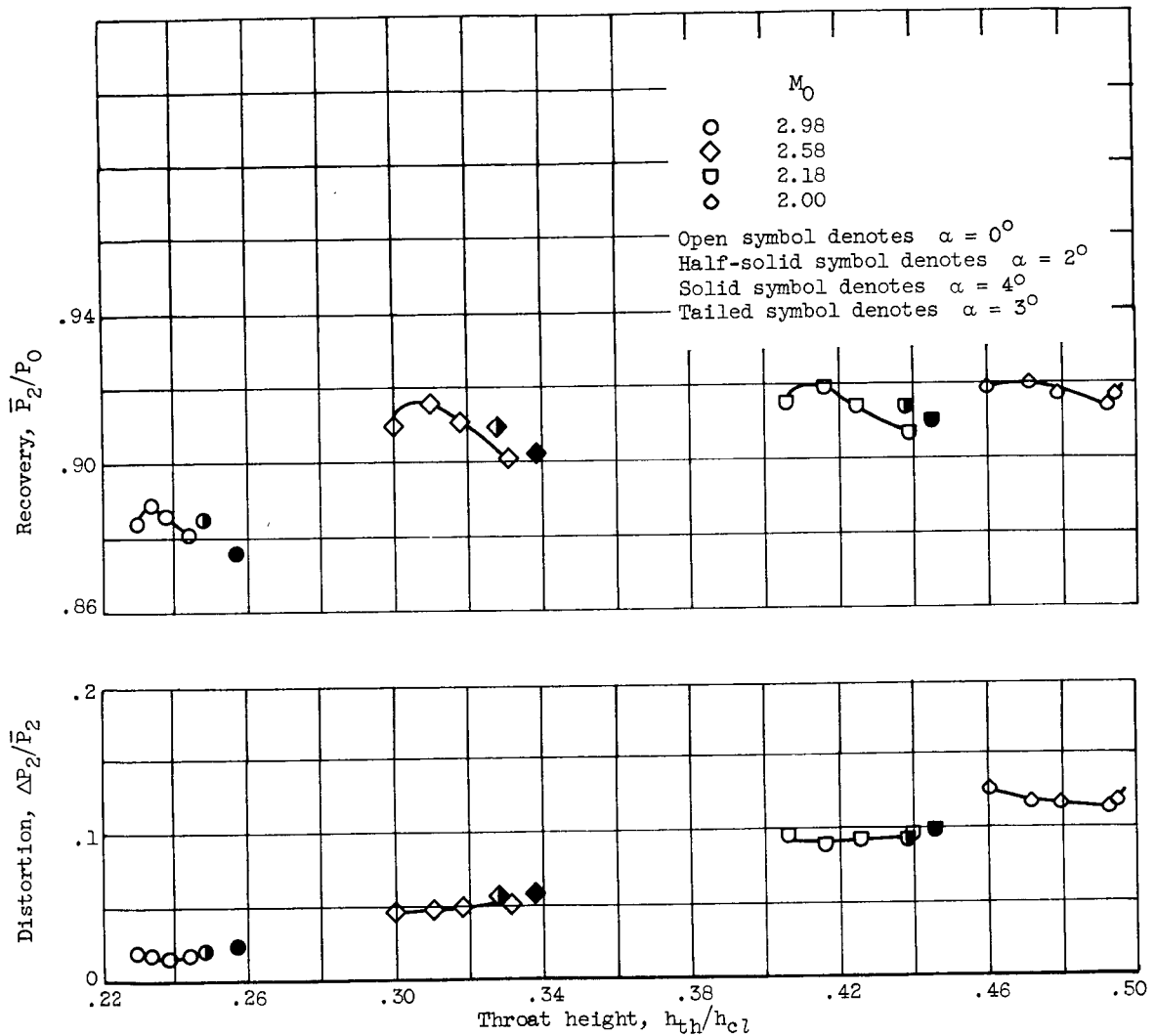
(b) Third-ramp angle, 15.5° (bypass closed but not sealed).

Figure 6. - Continued. Peak inlet performance. Reynolds number, 2.5×10⁶ per foot.
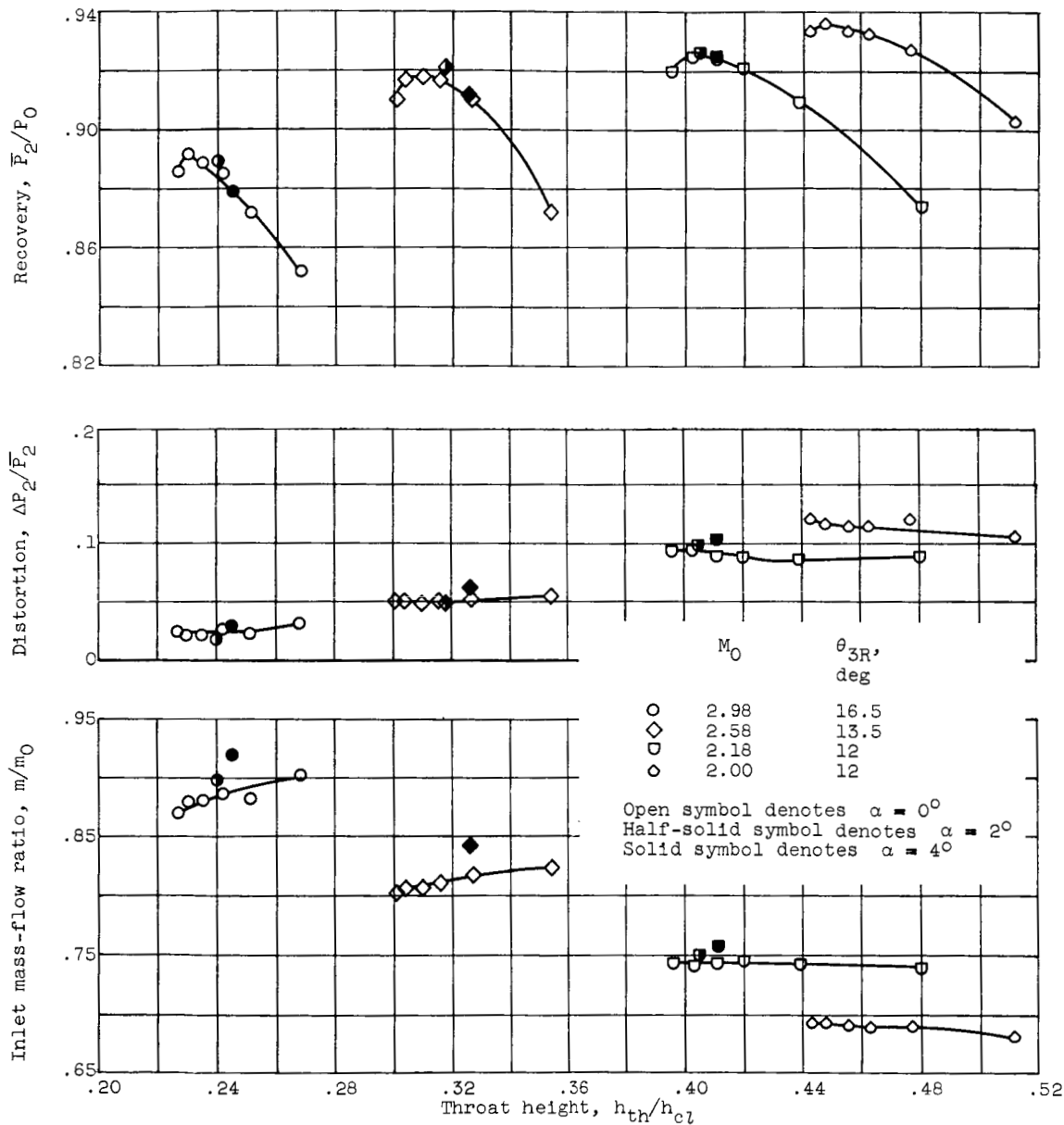
E-1073

(c) Third-ramp angle for maximum recovery (bypass sealed).

Figure 6. - Concluded. Peak inlet performance. Reynolds number, 2.5×10^6 per foot.
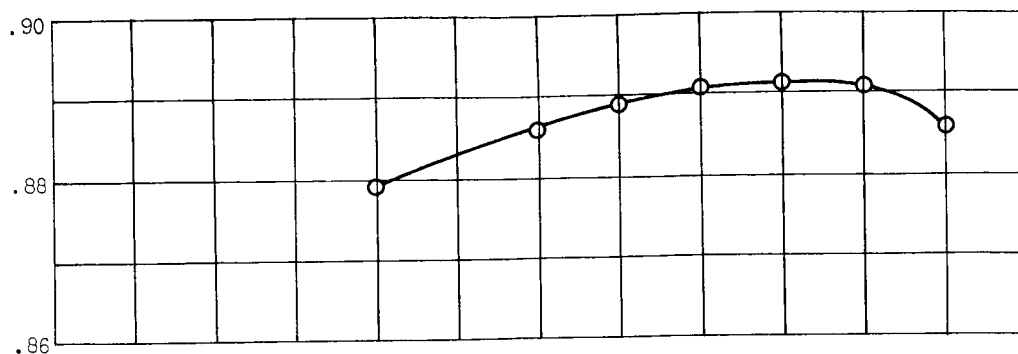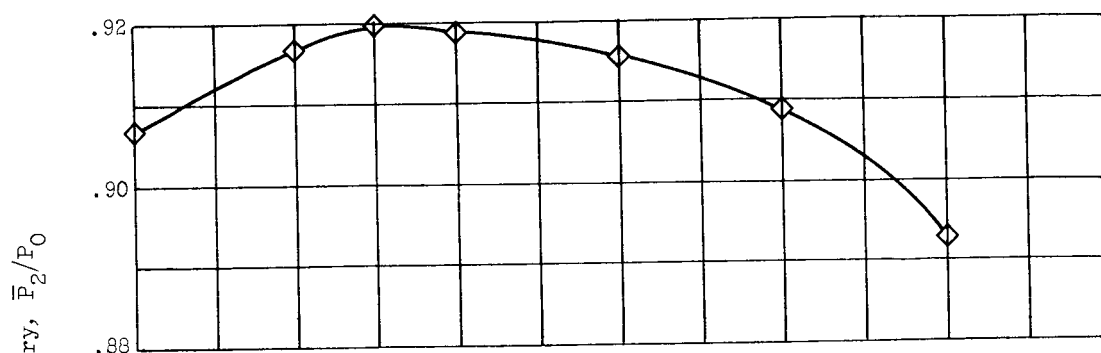
(a) Mach 2.98.

(b) Mach 2.58.
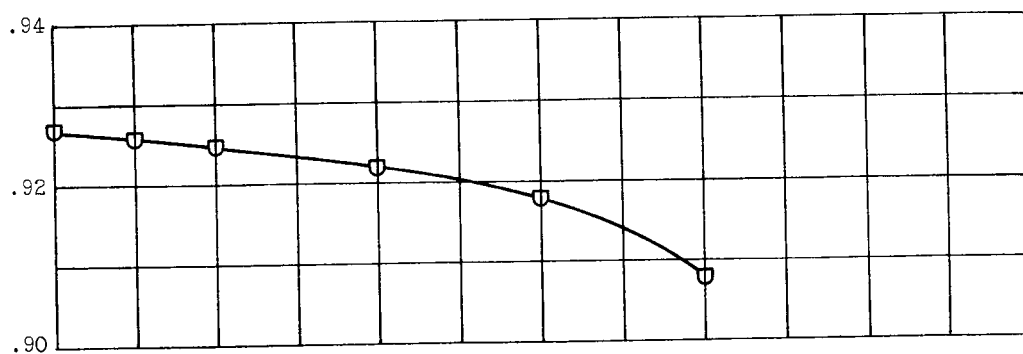
(c) Mach 2.18.
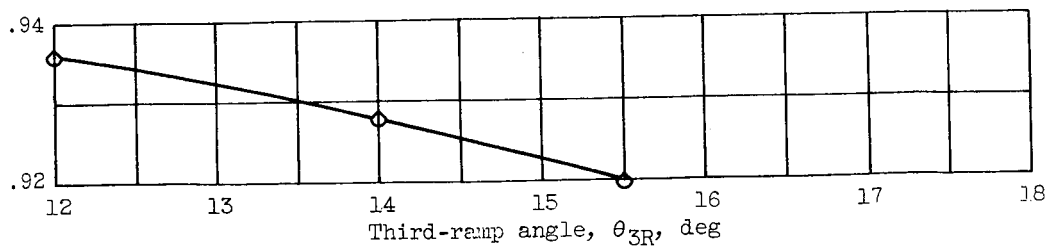
(d) Mach 2.00.

Figure 7. - Effect of third-ramp angle on inlet recovery at optimum throat height. Reynolds number, 2.5×10^6 per foot; angle of attack, $0°$.

DECLASSIFIED

E-1073
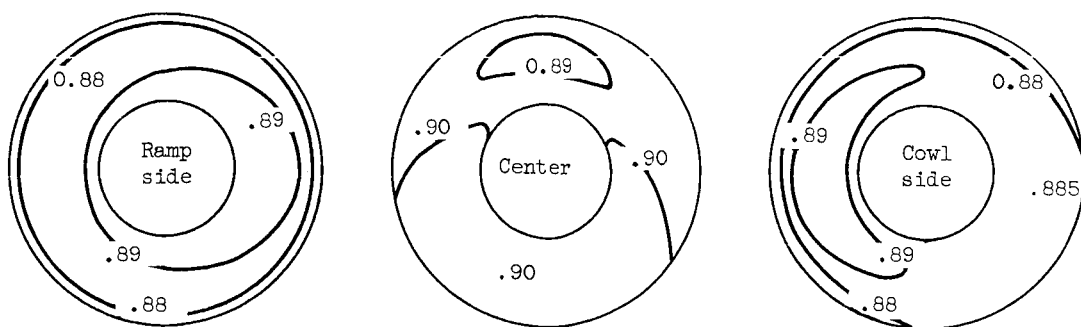
(a) Mach 2.98; third-ramp angle, 16.5°; bypass closed.
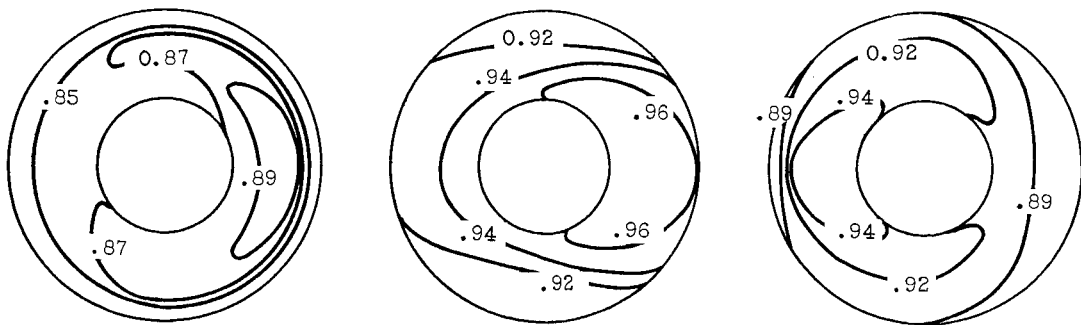
(b) Mach 2.18; third-ramp angle, 16.5°; bypass closed.
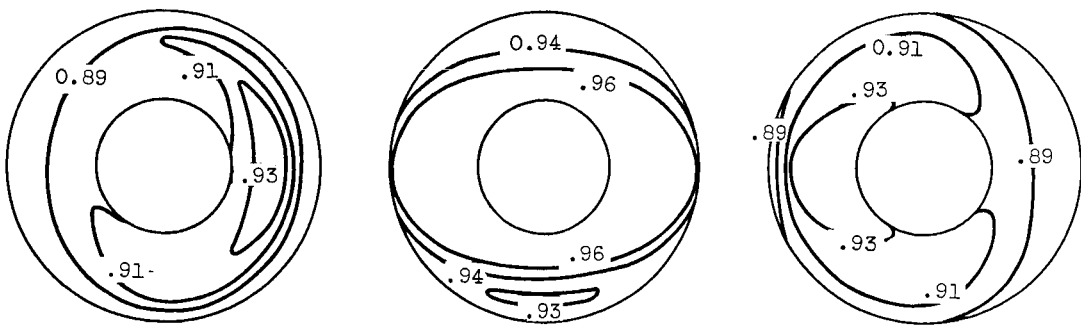
(c) Mach 2.18; third-ramp angle, 12°; bypass closed.
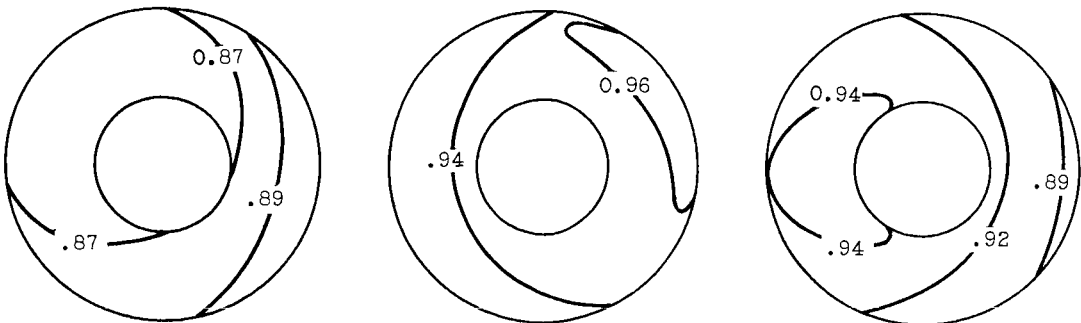
(d) Mach 2.18; third-ramp angle, 16.5°; bypass open to simulate typical
engine-face Mach numbers.

Figure 8. - Engine-face total-pressure recovery contours. Reynolds number, 2.5×10⁶ per
foot; angle of attack, 0°.
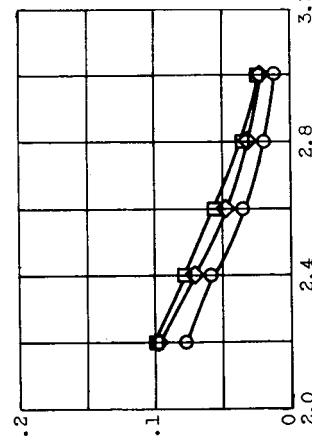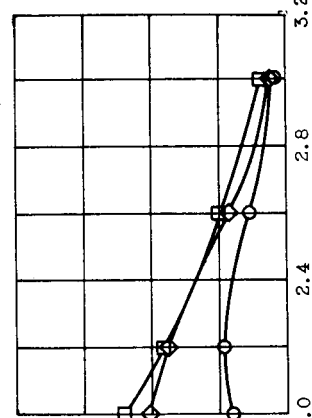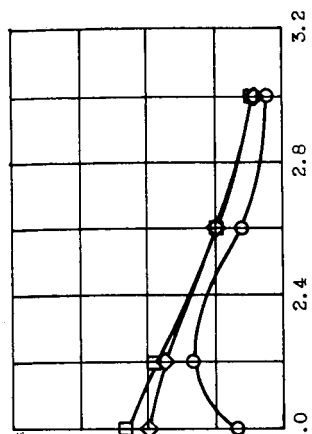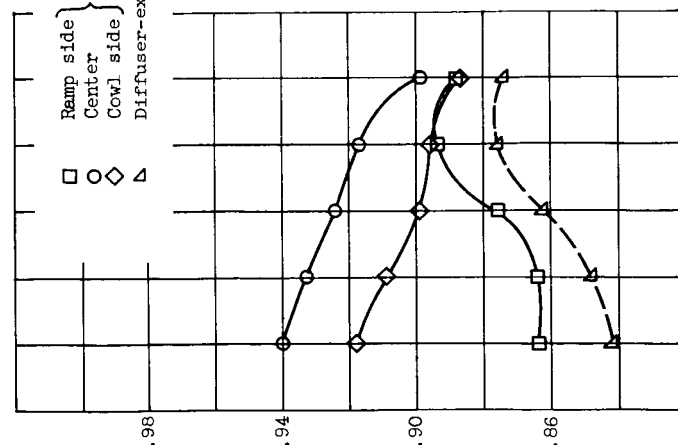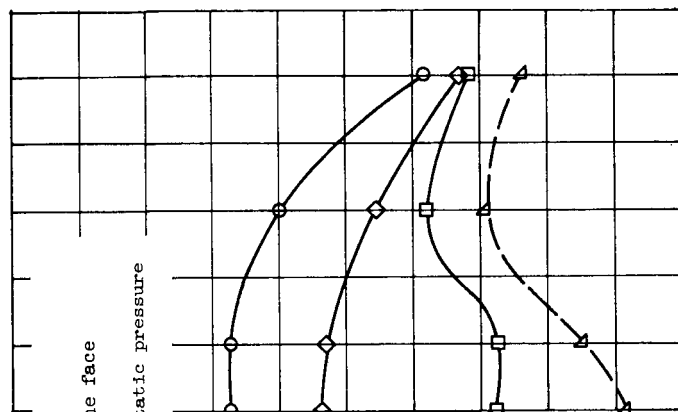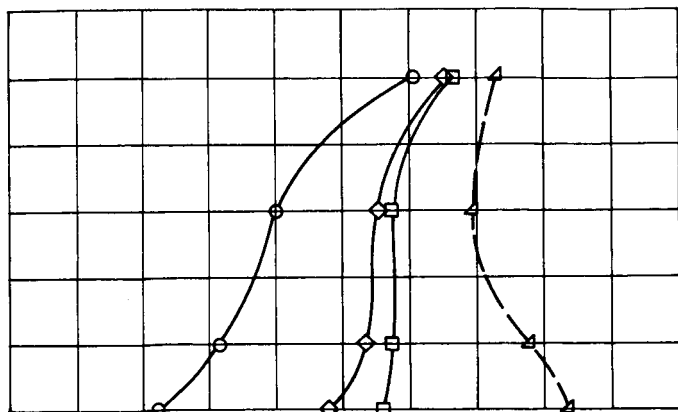
DECLASSIFIED

(c) Third-ramp angle for maximum recovery.

(b) Third-ramp angle, 15.5°.

(a) Third-ramp angle, 16.5°.

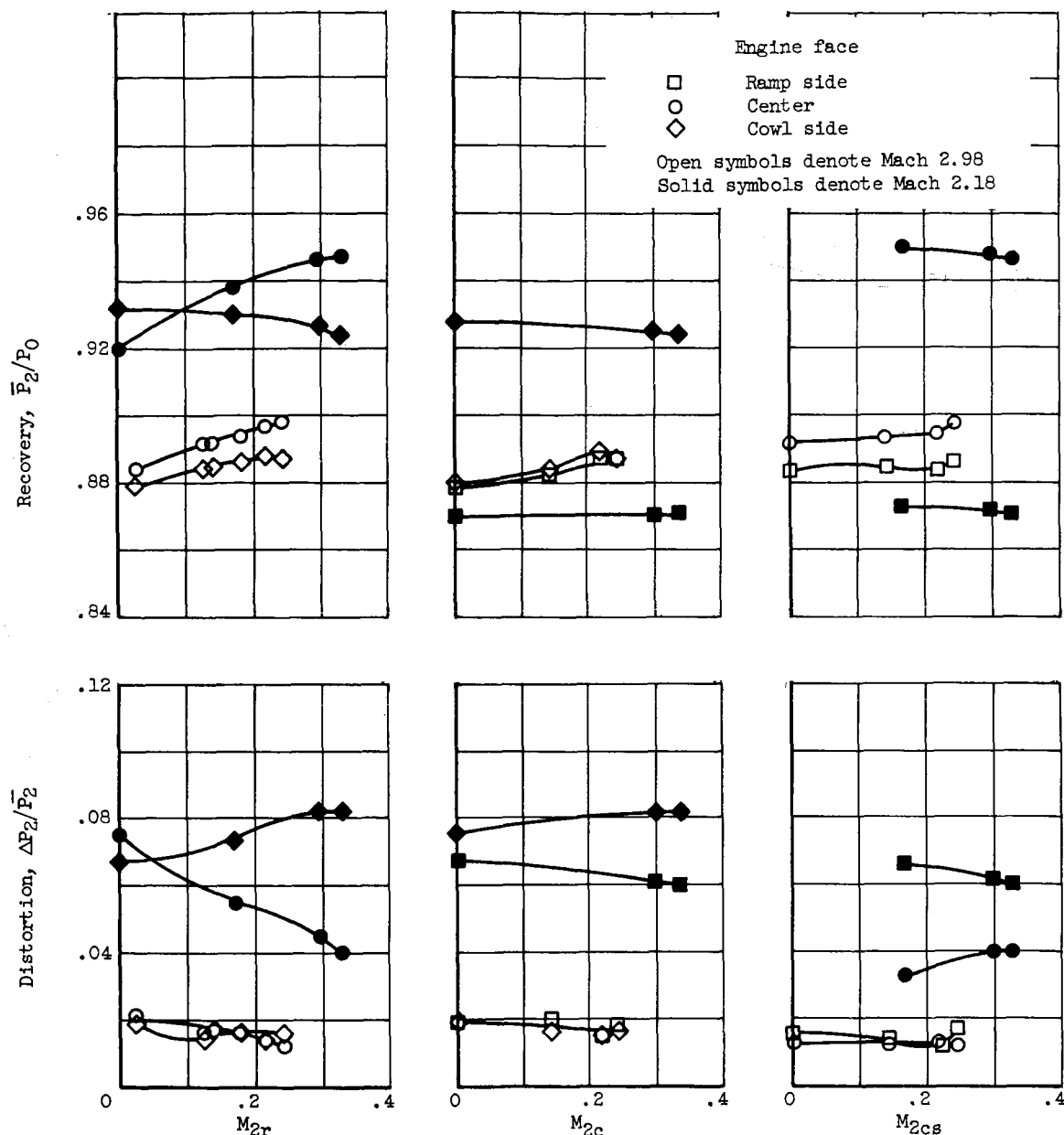Figure 9. – Individual engine-face peak performance. Reynolds number, 2.5×10^6 per foot; angle of attack, 0°.

E-1073

Engine face

☐ Ramp side
○ Center
◇ Cowl side

Open symbols denote Mach 2.98
Solid symbols denote Mach 2.18

(a) Simulation of ramp-side engine out. M_{2c} and M_{2cs} constant at maximum value of M_{2r}.

(b) Simulation of center engine out. M_{2r} and M_{2cs} constant at maximum value of M_{2c}.

(c) Simulation of cowl-side engine out. M_{2r} and M_{2c} constant at maximum value of M_{2cs}.

Figure 10. - Change in individual engine-face peak performance with alternate reduction in flow at each engine face, to simulate one-engine-out conditions. Third-ramp angle, 16.5°; angle of attack, 0°; Reynolds number, 2.5×10^6 per foot.
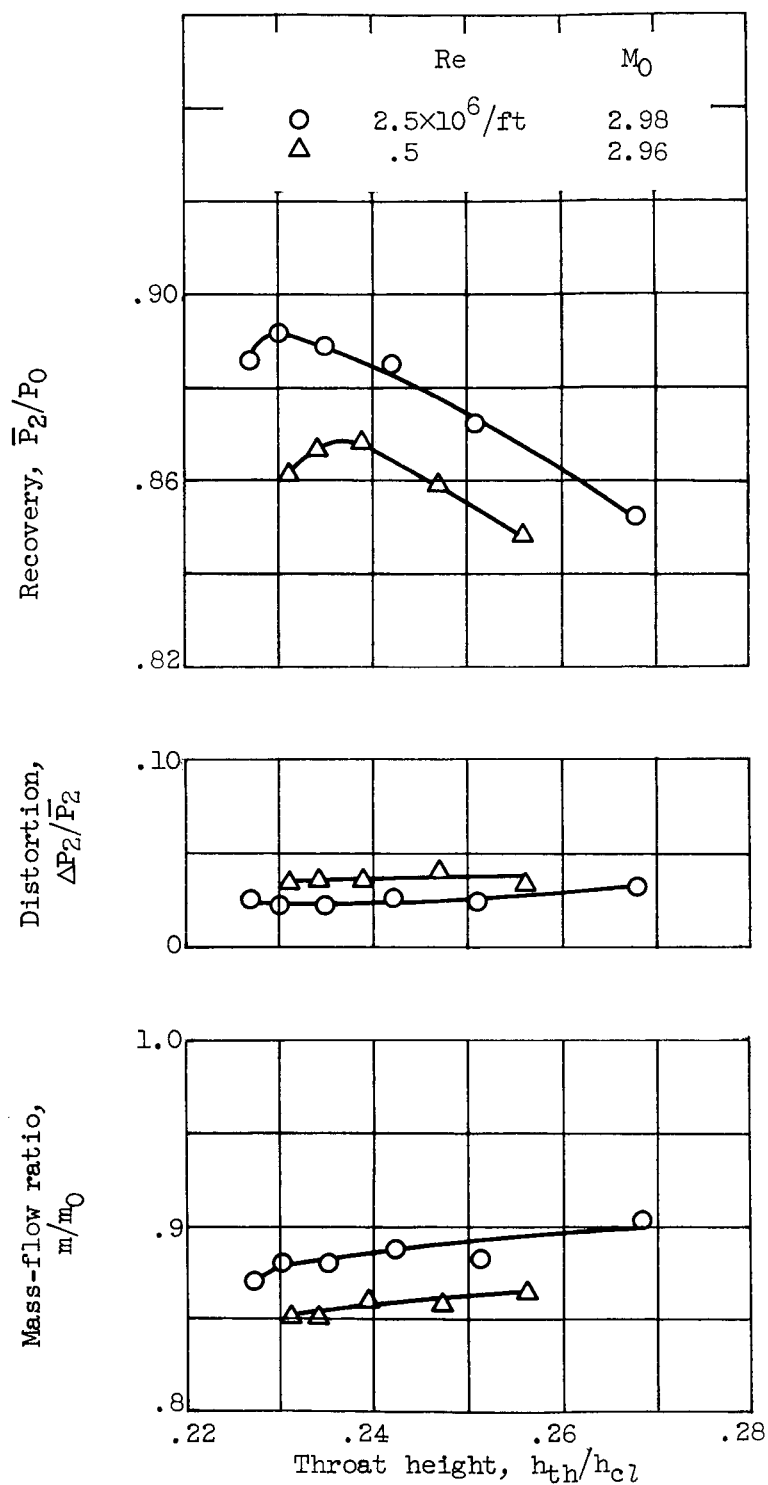
Figure 11. - Effect of Reynolds number on peak inlet performance. Angle of attack, 0°; third-ramp angle, 16.5°.
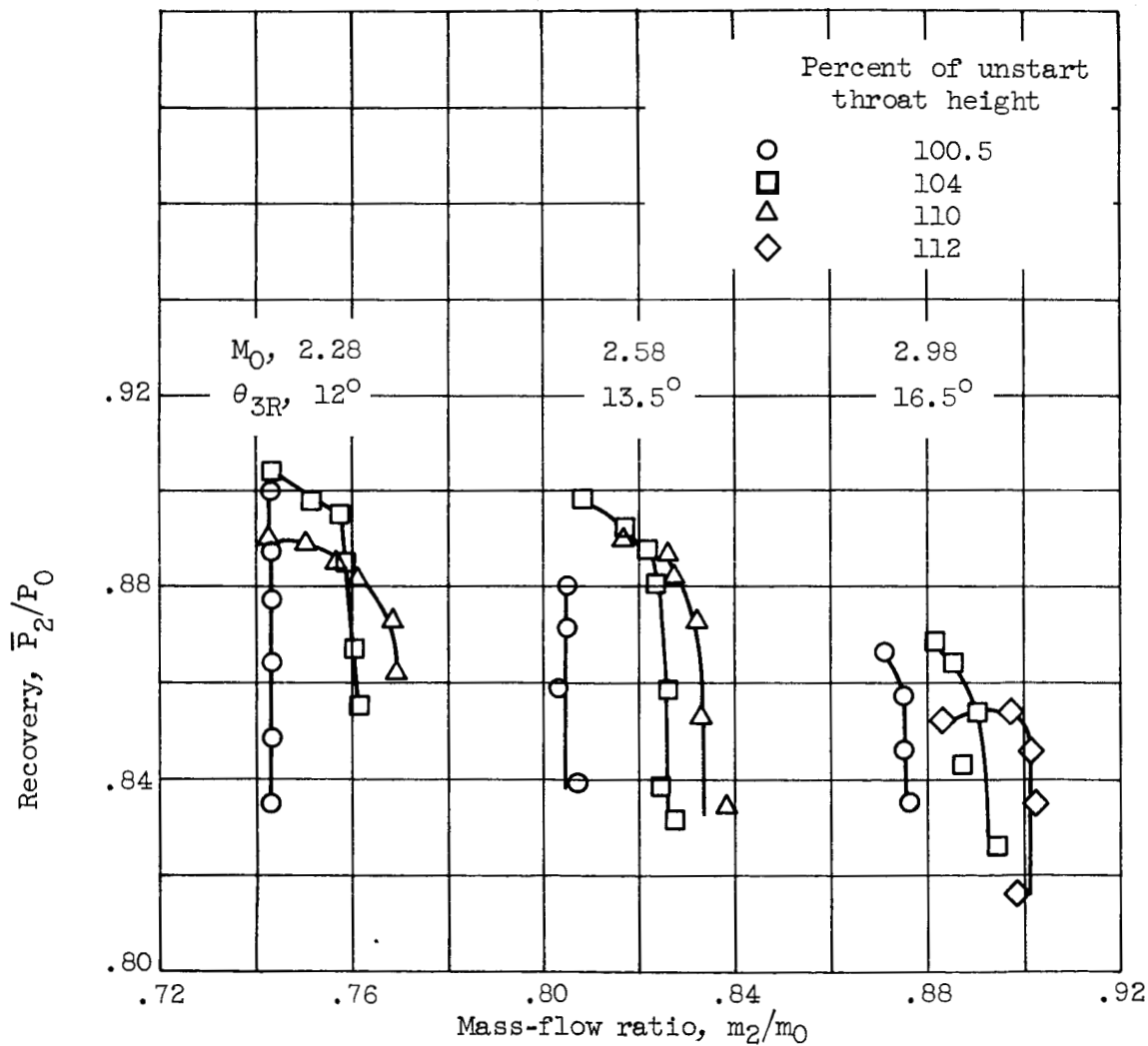
E-1073

Figure 12. - Variation in inlet mass-flow ratio with change in recovery at third-ramp angle for maximum recovery. Reynolds number, 2.5×10^6 per foot; angle of attack, 0°.
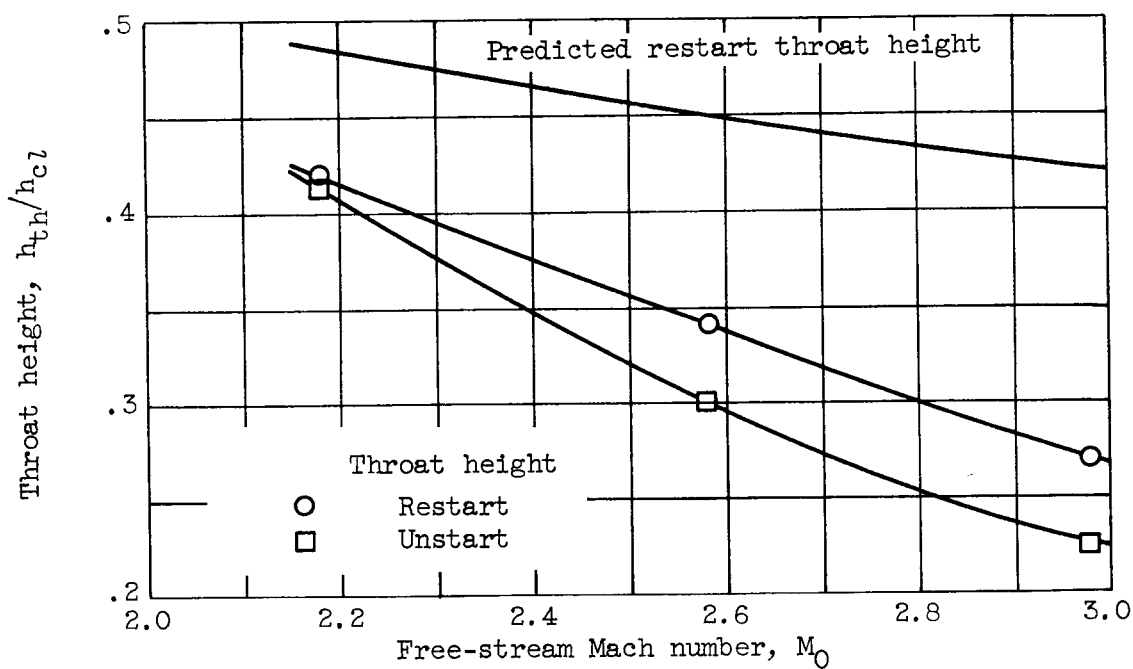
Figure 13. - Comparison of restart throat height with predicted value and unstart throat height. Third-ramp angle, 16.5°; Reynolds number, 2.5×10^{6} per foot.

E-1073
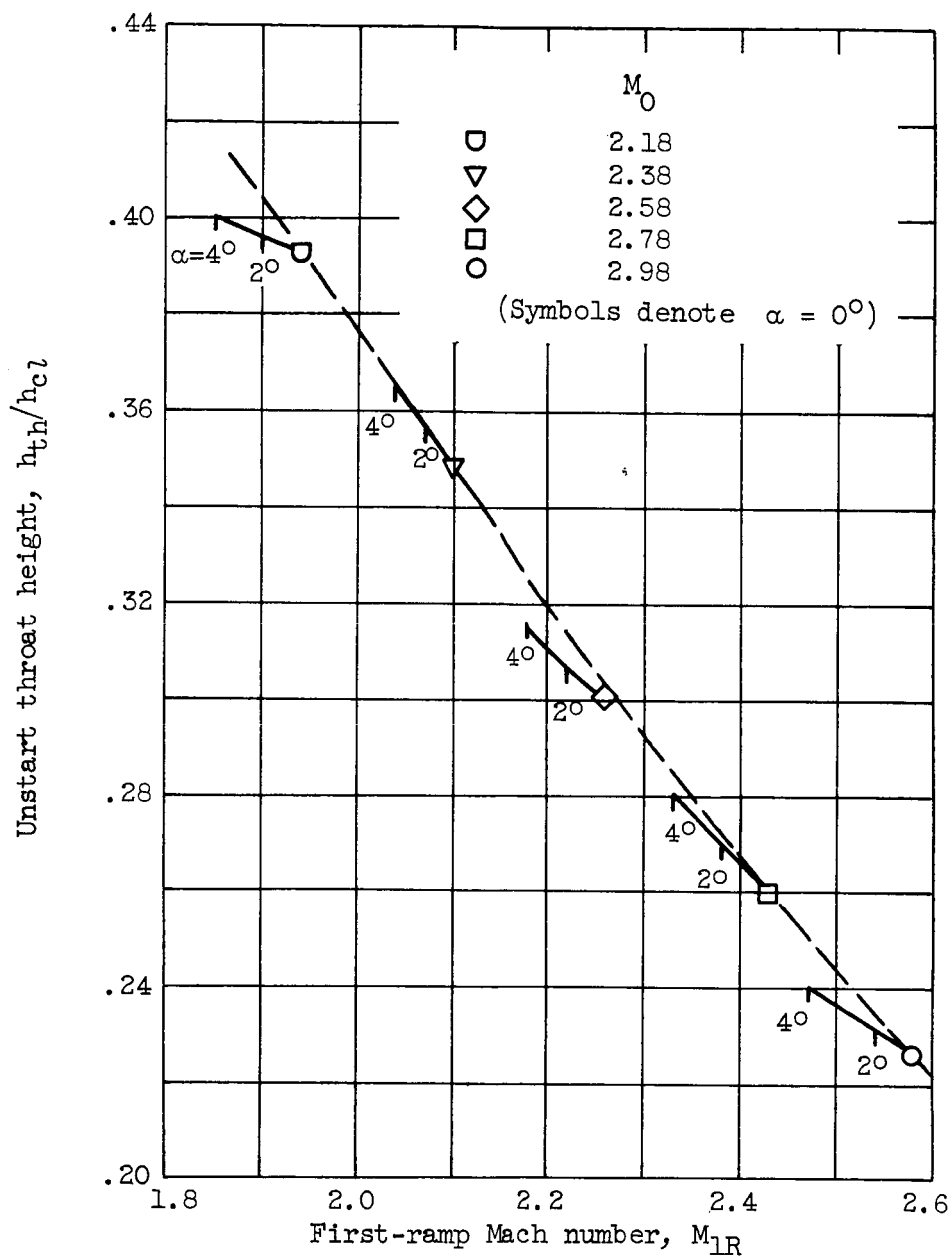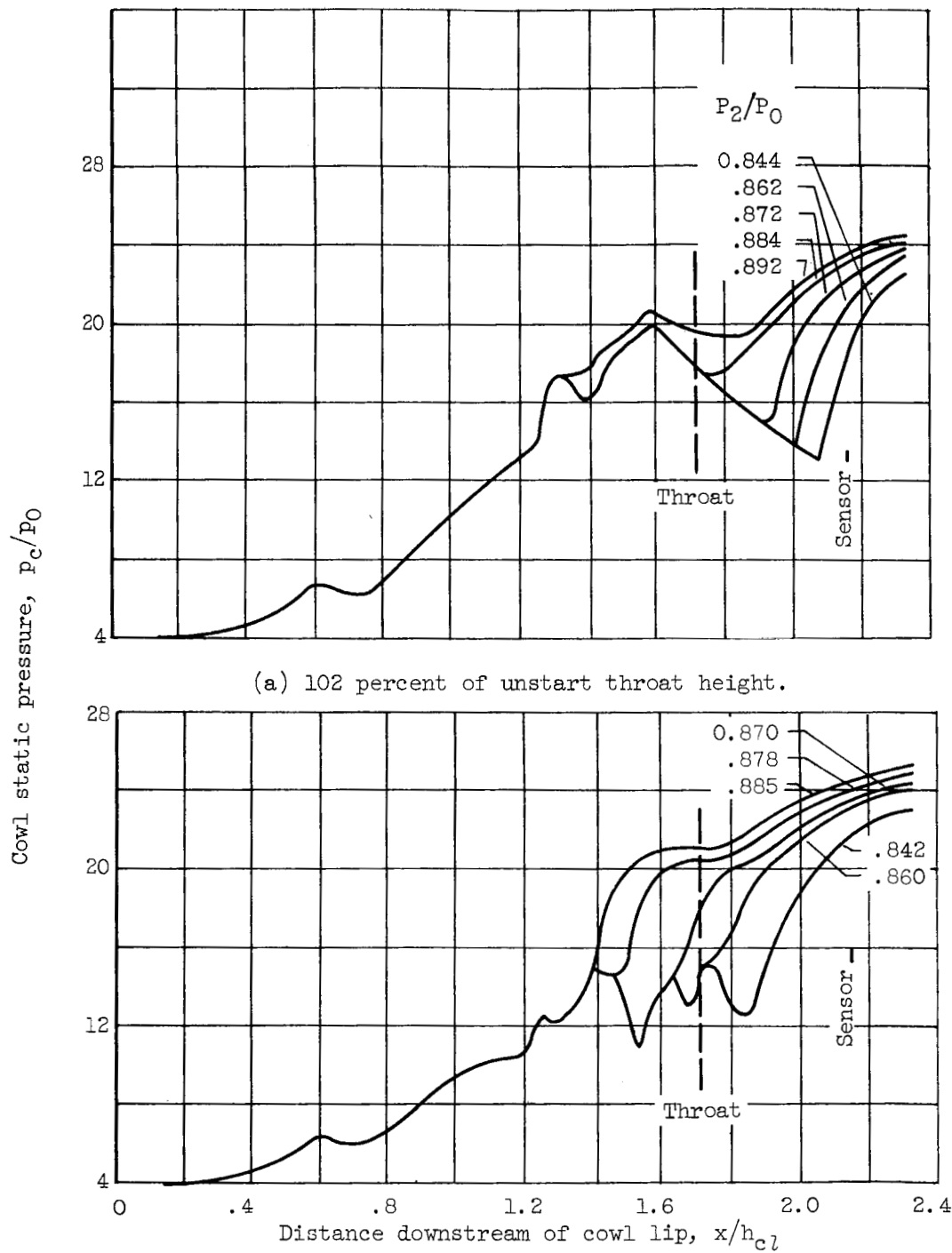

Figure 14. - Effect of first-ramp Mach number on un-
start throat height. First-ramp angle, 16.5°;
Reynolds number, 2.5×10⁶ per foot.

E-1073

(a) 102 percent of unstart throat height.

(b) 108 percent of unstart throat height.

Figure 15. - Cowl static-pressure distributions. Free-stream Mach number, 3.0; angle of attack, 0°; Reynolds number, 2.5×10^6 per foot.

E-1073
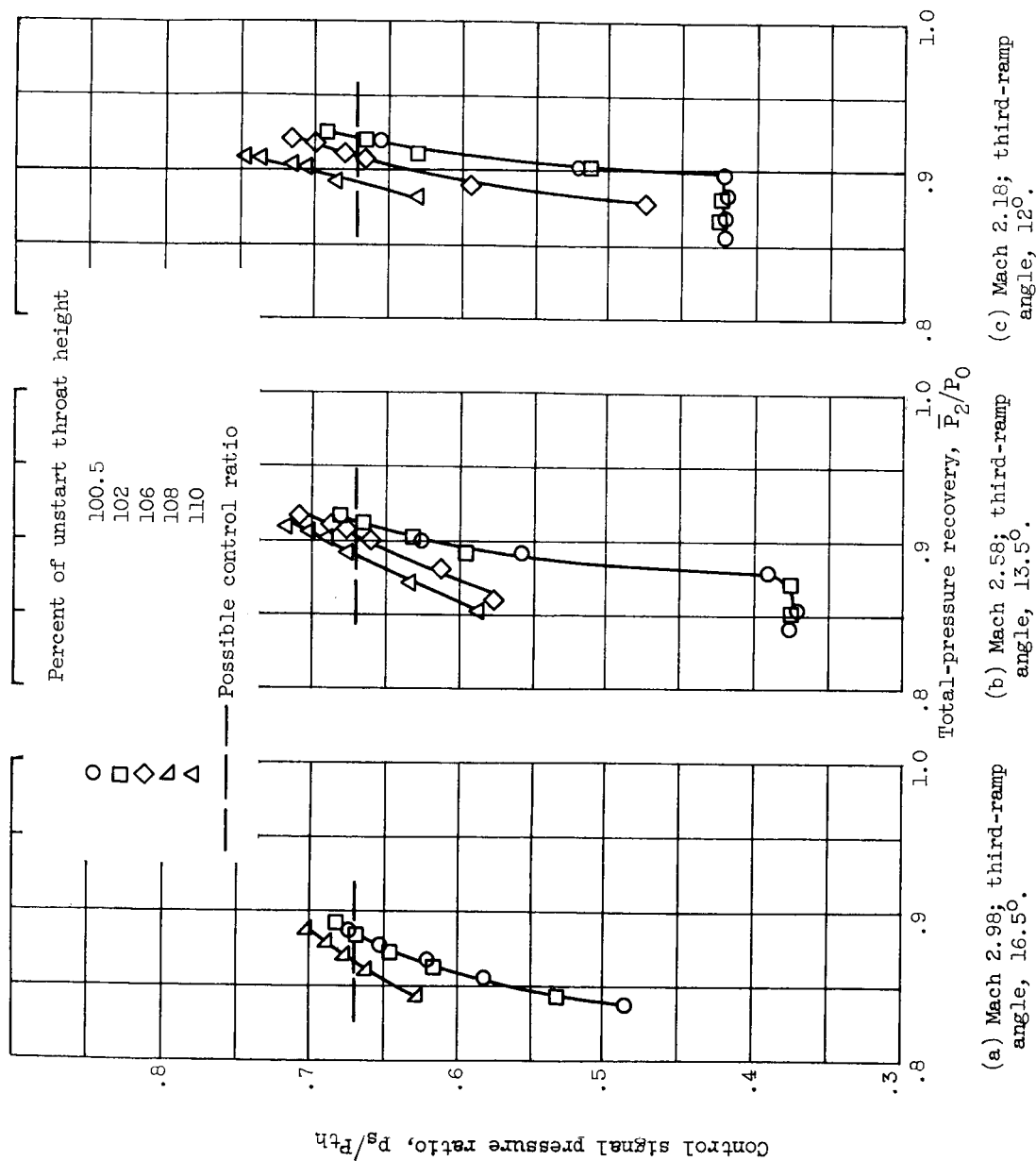

Figure 16. - Recovery control parameter performance at 0° angle of attack and third-ramp angle for maximum recovery.

(a) Mach 2.98; third-ramp angle, 16.5°.

(b) Mach 2.58; third-ramp angle, 13.5°.

(c) Mach 2.18; third-ramp angle, 12°.

E-1073
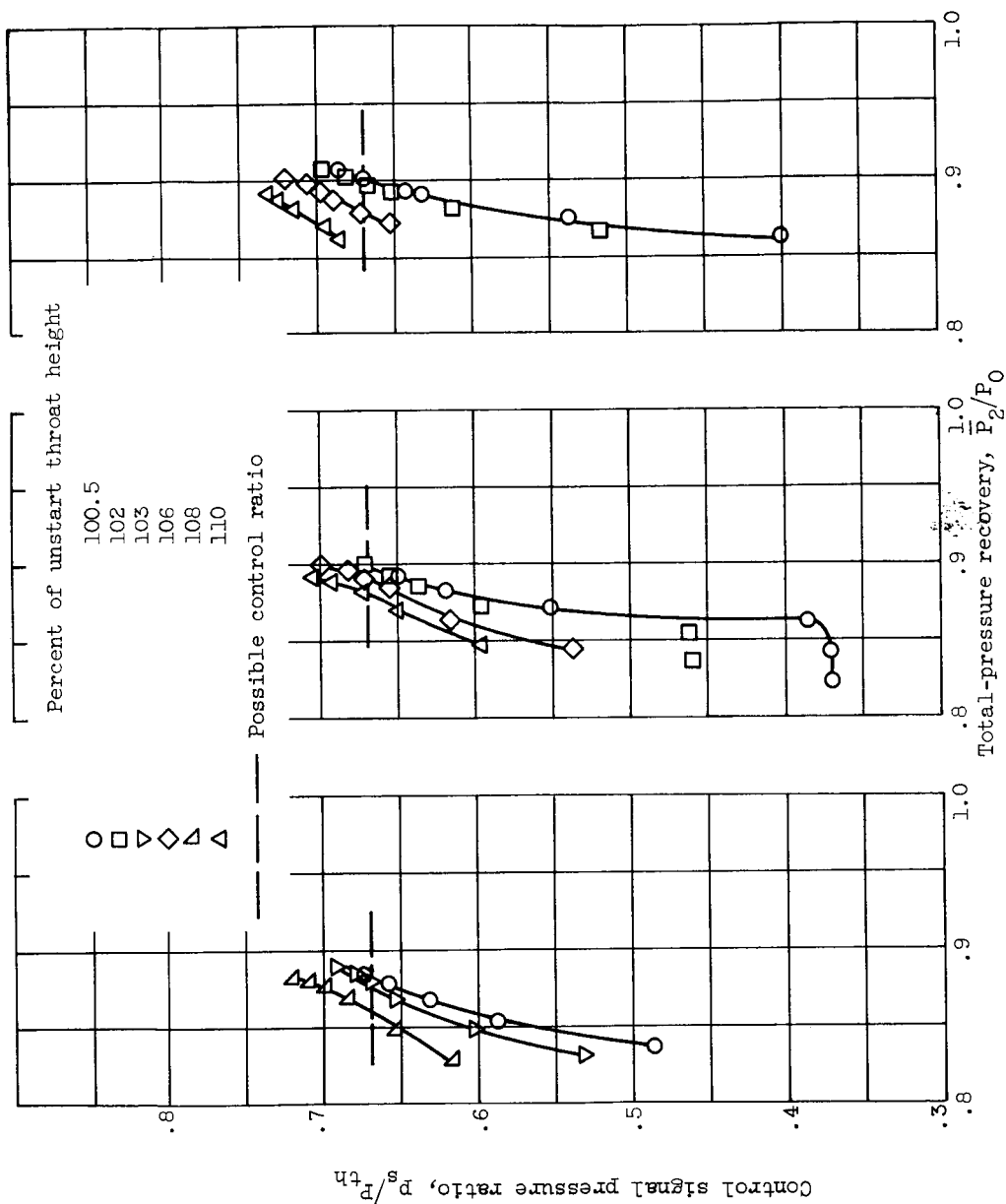

Figure 17. - Recovery control parameter performance at 0° angle of attack and third-ramp angles other than for maximum recovery.

(a) Mach 2.98; third-ramp angle, 15.5°.

(b) Mach 2.58; third-ramp angle, 16.5°.

(c) Mach 2.18; third-ramp angle, 16.5°.

E-1073

(a) Mach 2.98; third-ramp angle, 16.5°.

(b) Mach 2.58; third-ramp angle, 13.5°.
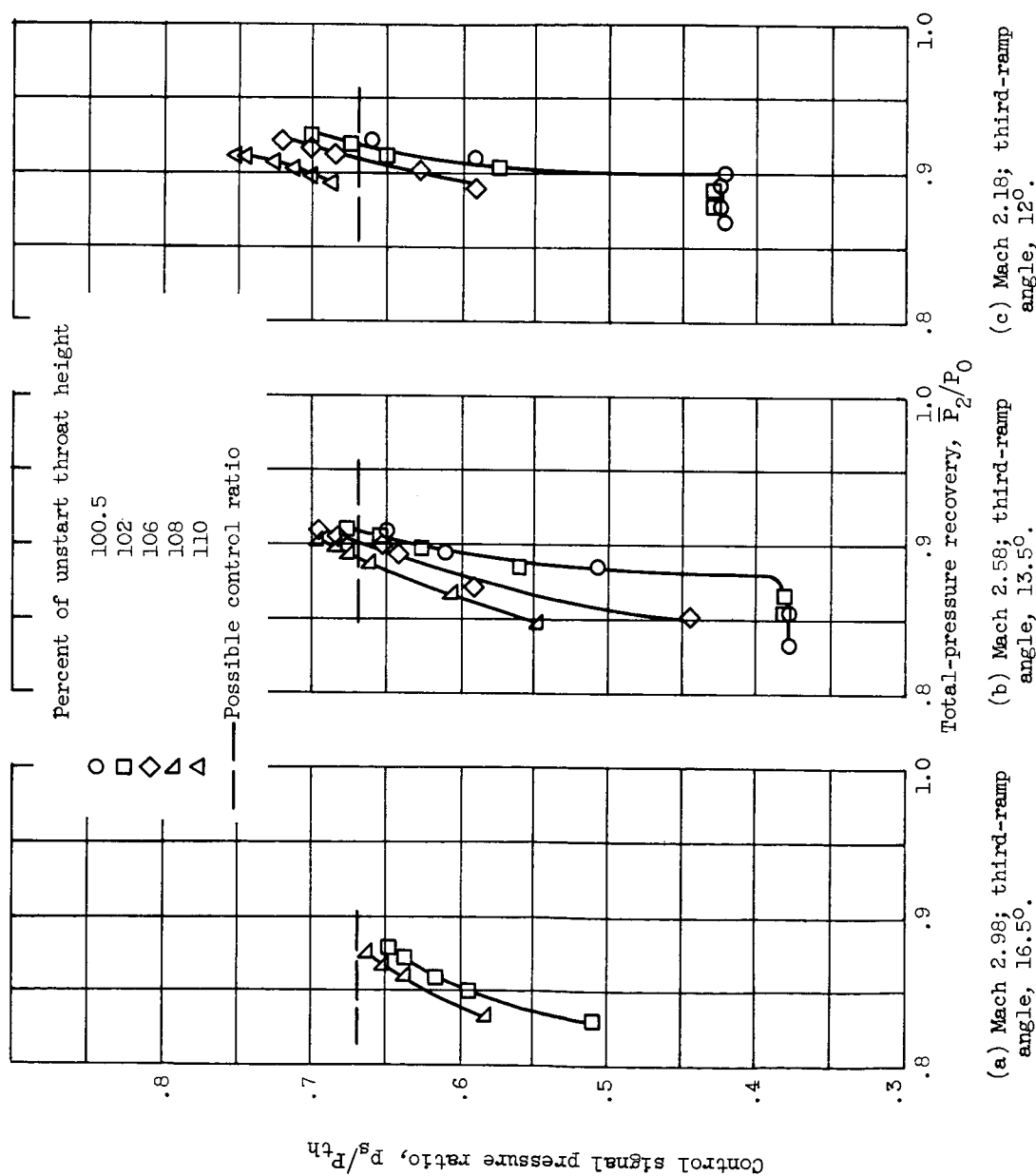
(c) Mach 2.18; third-ramp angle, 12°.

Figure 18. – Recovery control parameter performance at 4° angle of attack and third-ramp angle for maximum recovery.

DECLASSIFIED
CONFIDENTIAL
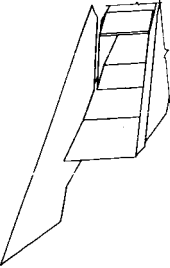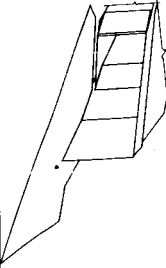
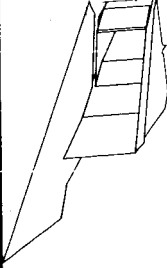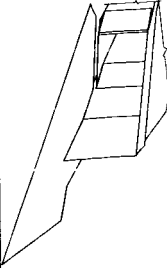NOTES: (1) Reynolds number is based on the diameter of a circle with the same area as that of the capture area of the inlet.

(2) The symbol * denotes the occurrence of buzz.

INLET BIBLIOGRAPHY SHEET

Report and facility	Description Configuration	Number of oblique shocks	Type of boundary-layer control	Free-stream Mach number	Reynolds number × 10⁻⁶	Angle of attack, deg	Angle of yaw, deg	Drag	Inlet-flow profile	Discharge-flow profile	Flow picture	Maximum total-pressure recovery	Mass-flow ratio	Remarks
CONFID. NASA TM X-470 Lewis 10-by 10-ft Super-sonic Wind Tunnel		4 from ramps that are inter-nally re-flected	Porous wall bleed	2.0 2.2 2.4 2.6 2.8 3.0	2.5 2.5 2.5 2.5 2.5 0.5,2.5	0,2,4 0,2,4 0,2,4 0,2,4 0,2,4	0	No	No	Yes		0.936 .926 .902 .918 .905 .892	0.693 .75 .770 .808 .855 .880	Overall performance, engine-out performance for three-engine configuration, and inlet-contraction and shock-position control parameters are presented.
CONFID. NASA TM X-470 Lewis 10-by 10-ft Super-sonic Wind Tunnel		4 from ramps that are inter-nally re-flected	Porous wall bleed	2.0 2.2 2.4 2.6 2.8 3.0	2.5 2.5 2.5 2.5 2.5 0.5,2.5	0,2,4 0,2,4 0,2,4 0,2,4 0,2,4	0	No	No	Yes		0.936 .926 .902 .918 .905 .892	0.693 .75 .770 .808 .855 .880	Overall performance, engine-out performance for three-engine configuration, and inlet-contraction and shock-position control parameters are presented.
CONFID. NASA TM X-470 Lewis 10-by 10-ft Super-sonic Wind Tunnel		4 from ramps that are inter-nally re-flected	Porous wall bleed	2.0 2.2 2.4 2.6 2.8 3.0	2.5 2.5 2.5 2.5 2.5 0.5,2.5	0,2,4 0,2,4 0,2,4 0,2,4 0,2,4	0	No	No	Yes		0.936 .926 .902 .918 .905 .892	0.693 .75 .770 .808 .855 .880	Overall performance, engine-out performance for three-engine configuration, and inlet-contraction and shock-position control parameters are presented.
CONFID. NASA TM X-470 Lewis 10-by 10-ft Super-sonic Wind Tunnel		4 from ramps that are inter-nally re-flected	Porous wall bleed	2.0 2.2 2.4 2.6 2.8 3.0	2.5 2.5 2.5 2.5 2.5 0.5,2.5	0,2,4 0,2,4 0,2,4 0,2,4 0,2,4	0	No	No	Yes		0.936 .926 .902 .918 .905 .892	0.693 .75 .770 .808 .855 .880	Overall performance, engine-out performance for three-engine configuration, and inlet-contraction and shock-position control parameters are presented.

Bibliography

These strips are provided for the convenience of the reader and can be removed from this report to compile a bibliography of NASA inlet reports. This page is being added only to inlet reports and is on a trial basis.

CONFIDENTIAL